Structure of high-resolution $K\beta_{1,3}$ x-ray emission spectra for the elements from Ca to Ge

Y. Ito,[1,*] T. Tochio,[2] M. Yamashita,[3] S. Fukushima,[4] A. M. Vlaicu,[5] Ł. Syrocki,[6] K. Słabkowska,[6] E. Weder,[6] M. Polasik,[6] K. Sawicka,[6] P. Indelicato,[7] J. P. Marques,[8,9] J. M. Sampaio,[10] M. Guerra,[9] J. P. Santos,[9] and F. Parente[9,8]

[1]*Laboratory of Atomic & Molecular Physics, ICR, Kyoto University, Gokasho, Uji, Kyoto 611-0011 Japan*
[2]*Department of Physics, Faculty of Science, Kobe University, 1-1 Rokkodai, Kobe 657-8501, Japan*
[3]*HIT, 3-1-12 Yukihira, Suma-ku, Kobe 654-0037, Japan*
[4]*Kobe Material Testing Laboratory Co., Ltd., NewSBARU, 1-1-2 Koto, Kamigori, Hyogo 678-1205, Japan*
[5]*National Institute of Materials Physics, Bucharest-Magurele, Atomistilor Strasse 405A, P.O. Box MG-7, 077125 Magurele-Ilfov, Romania*
[6]*Faculty of Chemistry, Nicolaus Copernicus University in Toruń, Gagarina7, 87-100 Toruń, Poland*
[7]*Laboratoire Kastler Brossel, Sorbonne Université, CNRS, ENS-PSL Research University, Collège de France, Case 74; Campus Pierre et Marie Curie, 4, Place Jussieu, F-75005 Paris, France*
[8]*BioISI-Biosystems & Integrative Sciences Institute, Faculdade de Ciências da Universidade de Lisboa, Campo Grande, C8, 1749-016 Lisboa, Portugal*
[9]*Laboratório de Instrumentação, Engenharia Biomédica e Física da Radiação (LIBPhys-UNL), Departamento de Física, Faculdade de Ciências e Tecnologia da Universidade Nova de Lisboa, Monte da Caparica, 2892-516 Caparica, Portugal*
[10]*LIP – Laboratório de Instrumentação e Física Experimental de Partículas, Av. Prof. Gama Pinto 2, 1649-003 Lisboa, Portugal*

(Received 18 January 2018; published 11 May 2018)

The $K\beta$ x-ray spectra of the elements from Ca to Ge have been systematically investigated using a high-resolution antiparallel double-crystal x-ray spectrometer. Each $K\beta_{1,3}$ natural linewidth has been corrected using the instrumental function of this type of x-ray spectrometer, and the spin doublet energies have been obtained from the peak position values in $K\beta_{1,3}$ x-ray spectra. For all studied elements the corrected $K\beta_1$ x-ray lines FWHM increase linearly as a function of Z. However, for $K\beta_3$ x-ray lines this dependence is generally not linear in the case of $3d$ elements but increases from Sc to Co elements. It has been found that the contributions of satellite lines are considered to be $[KM]$ shake processes. Our theoretically predicted synthetic spectra of Ca, Mn, Cu, and Zn are in very good agreement with our high-resolution measurements, except in the case of Mn, due to the open-shell valence configuration effect (more than 7000 transitions for diagram lines and more than 100 000 transitions for satellite lines) and the influence of the complicated structure of the metallic Mn.

DOI: 10.1103/PhysRevA.97.052505

I. INTRODUCTION

The $K\alpha$ and $K\beta$ x-ray emission spectra of the $3d$ transition metals exhibit several peculiar asymmetric line shapes not observed in other elements [1], whose origin has been under investigation and debate [2–5]. Several mechanisms such as shake-off and shake-up [6], conduction-band collective excitation [7], exchange [8], and final-state interactions [9] were suggested to account for this effect. However, recently, Deutsch *et al.* [4], Hölzer *et al.* [5], Anagnostopoulos *et al.* [10], Chantler *et al.* [11], and Ito *et al.* [12,13] suggested that the line shapes in $K\alpha_{1,2}$ x-ray spectra could be accounted for by the diagram transition, and $3s$, $3p$, and $3d$ spectator-hole transitions. Ito *et al.* [12] reported that the FWHM of the $K\alpha_{21}$ peak, which includes the satellite lines corresponding to the $K\alpha_2$ line, shows a different aspect from that of the $K\alpha_{11}$ peak, corresponding to a $K\alpha_1$ line, that may be ascribed to the L_2-$L_3M_{4,5}$ Coster-Kronig transitions. More recently, Ito *et al.* [13] measured systematically the $K\alpha_{1,2}$ spectra in the elements from Ca to Ge using an antiparallel two-crystal x-ray spectrometer and elucidated the origin of the asymmetry in the $K\alpha_1$ emission profile, confirming that the broadening of the linewidths of $K\alpha_2$ spectra originates from L_2-$L_3M_{4,5}$ Coster-Kronig transitions. Combined *ab initio* Dirac-Fock calculations and high-resolution x-ray emission measurements of $K\alpha_{1,2}$ spectra for Ca, Ti, and Ge elements show that the asymmetric line shapes of these emission lines can be fully explained by considering only the diagram and the $3d$ spectator transitions [13]. This interpretation can be also extended to other $3d$ transition metals.

The $K\beta_{1,3}$ x-ray emission spectrum includes $K\beta'$ and $K\beta''$ satellites on the low- and high-energy side of the $K\beta_{1,3}$ peak position, respectively, as explained in the case of copper [4]. These satellites have also been investigated until now both experimentally and/or theoretically [1,5,10,14–18] for all $3d$ transition metals. Shake-up from the $3d$ shell was also shown to account reasonably well for the measured $K\beta_{1,3}$ line shape, although a complete quantitative fitting has not been reported and possible contributions from other shells were not investigated [14,17]. The low-energy satellite group, denoted by $K\beta'$, received special attention, and several other sources such as exchange interaction [8] and plasmon oscillations [9] were suggested as its origin. It has been assumed that the line shape can be fully accounted for by satellites resulting from 3ℓ spectator holes in addition to the nominal single-electron

*Corresponding author: yoshito@scl.kyoto-u.ac.jp

TABLE I. Experimental conditions of the measurements using a two-crystal x-ray spectrometer. The measurements were done with a tube voltage of 40 kV and the current of 60 mA under vacuum. The step used $2\theta = 0.001^\circ$. The analyzing crystal was Si(220).

Element	Specimen	Line	Accumulation time (s/point)
Ca ($Z = 20$)	CaF_2	$K\beta_{1,3}, K\beta_5$	85
Sc ($Z = 21$)	Metal	$K\beta_{1,3}, K\beta_5$	75
Ti ($Z = 22$)	Metal	$K\beta_{1,3}, K\beta_5$	75
V ($Z = 23$)	Metal	$K\beta_{1,3}, K\beta_5$	75
Cr ($Z = 24$)	Metal	$K\beta_{1,3}, K\beta_5$	60
Mn ($Z = 25$)	Metal	$K\beta_{1,3}, K\beta_5$	50
Fe ($Z = 26$)	Metal	$K\beta_{1,3}, K\beta_5$	50
Co ($Z = 27$)	Metal	$K\beta_{1,3}, K\beta_5$	50
Ni ($Z = 28$)	Metal	$K\beta_{1,3}, K\beta_5$	50
Cu ($Z = 29$)	Metal	$K\beta_{1,3}, K\beta_5$	40
Zn ($Z = 30$)	Metal	$K\beta_{1,3}$	30
Ge ($Z = 32$)	Metal	$K\beta_{1,3}$	40
Ge ($Z = 32$)	Metal	$K\beta_{1,3}, K\beta_5$	50

diagram transitions. Recently, Limandri *et al.* [19] reported that the peak in the low-energy side of the $K\beta_{1,3}$ lines in Cr and Ni is due to the radiative Auger effect (RAE) of K-$M_{2,3}M_{4,5}$.

In the present work we performed a detailed systematic analysis of the $K\beta$ x-ray emission spectra for elements from Ca to Ge using the simple Lorentzian model [12,13] in order to elucidate the spin doublet energies of the $K\beta_{1,3}$ spectra and the satellite contribution of the $[KM]$ shake process. Moreover, we have evaluated theoretically the $[KM]$ shake processes and the M_2-$M_{4,5}M_{4,5}$, M_3-$M_{4,5}M_{4,5}$, and M_2-$M_3M_{4,5}$ super–Coster-Kronig transitions for the $K\beta$ emission spectra in elements from Ca to Ge. We have also compared the shapes of the theoretically predicted $K\beta_{1,3}$ x-ray spectra for Ca, Mn, Cu, and Zn elements, obtained as a superposition of contributions corresponding to diagram and M-shell satellite lines (the latter resulting from the creation of particular M-subshell holes), with the measured high-resolution x-ray spectra structures.

We also calculated the lifetime $K\beta_{1,3}$ linewidths for five $3d$ elements and the corresponding energy split.

II. EXPERIMENTAL METHODOLOGY

In the present work we used a Rigaku (3580EKI) double-crystal spectrometer. The experimental conditions for the measurements are given in Table I. Using Bragg reflections with this spectrometer, the true FWHM of the emission line can be determined by a simple subtraction of the convolution in the crystal dispersion from the FWHM of the measured emission line [20] (see Ref. [13] for details). With a Rh end-window x-ray generator operating at 40 kV, 60 mA, the emitted $K\beta$ spectra in elements from Ca to Ge (see Figs. 1 and 2) were recorded with a sealed Xe gas proportional counter in the symmetric Si (220) Bragg reflection of the double-crystal spectrometer at an angular step of 0.001 degrees in 2θ. The vertical divergence slit is 0.573 degrees in this spectrometer. Acquisition time was 50–85 s/point (see Table I). Neither smoothing nor correction was applied to the raw data. Each spectrum was repeated three times. The energy values of Bearden [21] were taken as starting points for the diagram line fitting parameters. We used CaF_2 crystal powder for Ca, metal foils for Sc, V, and Co, and metal plates for Ti, Mn, Fe, Cu, Zn, and Ge, respectively.

III. THEORETICAL BACKGROUND

A. Relativistic MCDF calculations

Theoretical predictions of the shape of the $K\beta_{1,3}$ x-ray diagram and satellite lines have been performed using the multiconfiguration Dirac-Fock (MCDF) method, which is the primary theoretical tool applied in atomic physics. Thanks to the ease of performing large-scale calculations, it is even possible to include electron correlations [22–29] to a large extent. The MCDF method allows for the determination of many of the significant atomic parameters, such as the structure of the energy levels and the level widths corresponding to the studied transitions. Our calculations have been done with the GRASP (General-Purpose Relativistic Atomic Structure Package) package [23,25,26], and with the Relativistic General Purpose Multiconfiguration Dirac-Fock code (MCDFGME) developed by Desclaux and Indelicato [28,29].

The MCDF method is described in detail in many papers [22–29]. The approximate relativistic Hamiltonian for an N-electron atom is taken in the form

$$\widehat{H} = \sum_{i=1}^{N} \hat{h}_D(i) + \sum_{j>i=1}^{N} V_B(i,j), \tag{1}$$

where $\hat{h}_D(i)$ is one-electron Dirac Hamiltonian, and $V_B(i,j)$ describes the sum of Coulomb repulsion and Breit interaction between the ith and the jth electron. In the MCDF method the wave function describing an N-electron atomic state, characterized by the quantum numbers J (determining the value of the total angular momentum) and M (determining the value of the projection of the total angular momentum on the quantization axis), and parity p, is assumed in the form [22]

$$\Psi_s(JM^p) = \sum_m c_m(s)\Phi(\gamma_m JM^p), \tag{2}$$

where $\Phi(\gamma_m JM^p)$ are N-electron configuration state functions (CSFs) built from one-electron Dirac spinors, $c_m(s)$ are the configuration mixing coefficients for state s, and γ_m contains all information necessary to uniquely define the respective CSFs.

The need of applying the MCDF method to these calculations is a consequence of the fact that in the case of open-shell states a given nonrelativistic configuration corresponds, usually, to several relativistic configurations. Therefore, to correctly describe an N-electron atomic state with a given set of quantum numbers and parity p, the intermediate coupling scheme must be used and the $\Psi_s(JM^p)$ function must be represented as a combination of $\Phi(\gamma_m JM^p)$ wave functions, according to Eq. (2). In the calculation of the x-ray spectra structure, all the states (whichever values of quantum numbers they have) corresponding to the set of initial configurations and all the states corresponding to the set of final configurations are simultaneously taken into account [24]. It is worth mentioning that the application of the relativistic MCDF method, taking into account Breit interaction and two quantum

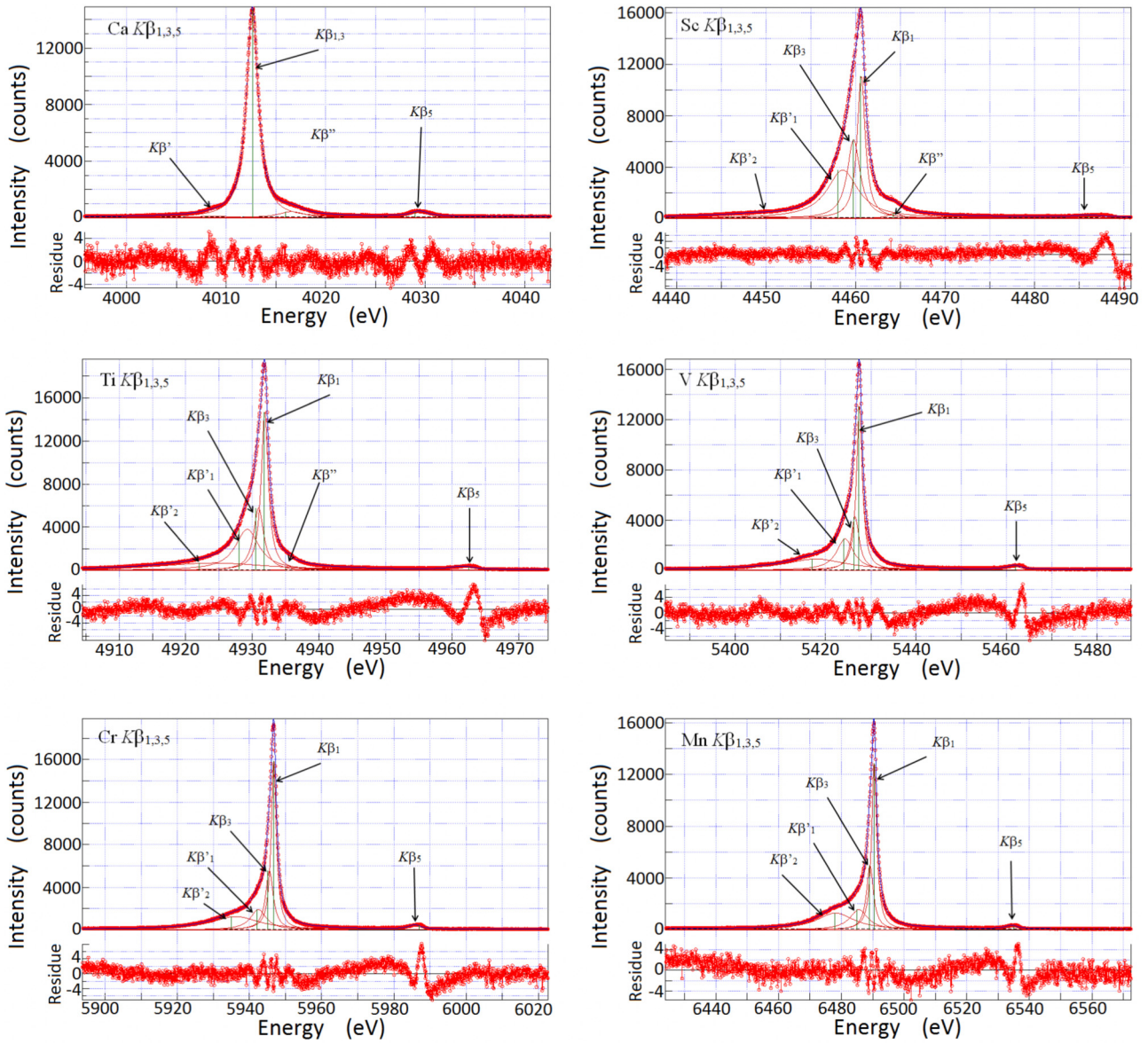

FIG. 1. The observed $K\beta_{1,3}$ spectra in elements Ca to Mn are shown with the fitting Lorentzian functions. These spectra were measured using the antiparallel double-crystal x-ray spectrometer described in detail in Ref. [13]. In this figure, the $K\beta''$ line is a satellite line resulting from a $3p$ spectator hole (see Ref. [11] and references therein).

electrodynamics corrections (so-called QED corrections: self-energy and vacuum polarization) is crucial to reliably determine the significant atomic parameters with the highest possible accuracy.

The calculations of radiationless super–Coster-Kronig transitions for all studied elements have been carried out by means of the Flexible Atomic Code (FAC) [30], which is based on a modified Dirac-Fock-Slater (DFS) method [31]. In general, the multiconfiguration DFS method is similar to the MCDF method, but a simplified expression for the electronic exchange integrals is used.

B. Electron shake probabilities in sudden approximation

The ejection of an inner-shell electron in an atomic system may lead to the excitation of outer-shell electrons to higher bound levels or to the continuum. These processes of additional monopole excitation and ionization are called shake processes, and they have been studied since the 1940s by Feinberg [32] and Migdal [33]. They give rise to intense satellite structures in all the inner-shell spectroscopic experiments (x-ray emission, x-ray absorption, Auger, and photoelectron spectra). Nowadays, unlike in the early studies in which all the shake processes were called shake-off, one distinguishes between the shake-up (SU) and the shake-off (SO) processes. In the SU processes an electron is excited into the bound states, while in the SO processes it is ejected into the states of the continuous spectrum.

The perturbative character of the SO and SU mechanism allows us to apply the so-called sudden approximation (SA) [34] for high-energy incident particles (photons or electrons). In this approach, the shake mechanism is described as a two-step process, where in the first step the photoelectron is ejected

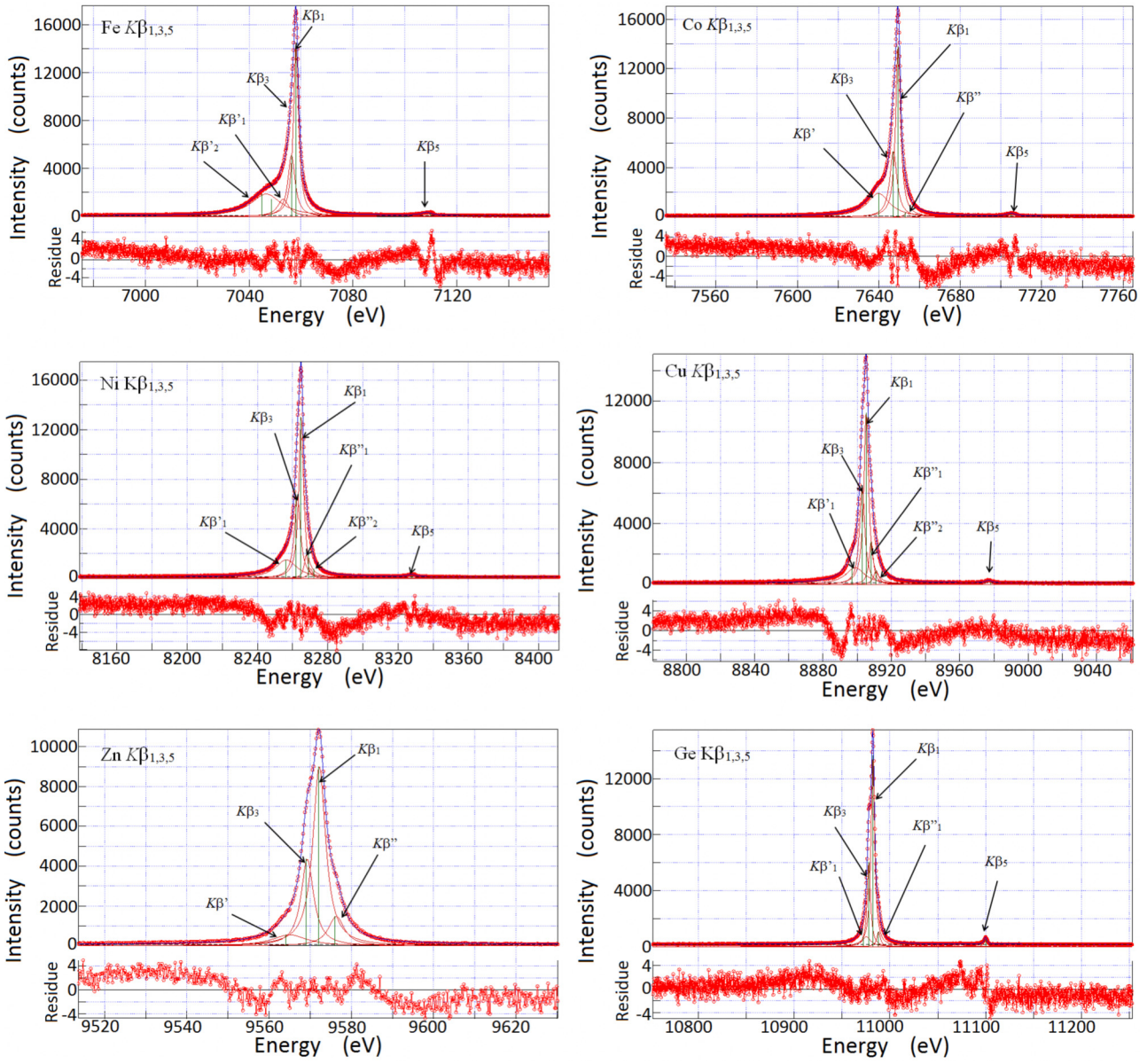

FIG. 2. The observed $K\beta_{1,3}$ spectra in elements Fe to Ge are shown with the fitting Lorentzian functions. These spectra were measured using the antiparallel double-crystal x-ray spectrometer described in detail in Ref. [13]. In this figure, the $K\beta''$ line is a satellite line resulting from a $3d$ spectator hole (see Ref. [4] and references therein).

and in the second step the remaining electrons experience an electrostatic potential change such that the projection of the initial electron wave function on the final wave functions governs the shake probabilities. The experimental results of Carlson and Krause [35] and Carlson *et al.* [36], as well as theoretical predictions of Krause and Carlson [37], Sachenko and Burtsev [38], Santos *et al.* [39], and Mauron *et al.* [40], support the validity of this approximation for atomic excitation following inner-shell vacancy production.

The SO and SU probability for removing one or more electrons from an orbital $|\psi_{n\ell j}\rangle$, where n and ℓ are the principal and orbital angular-momentum quantum numbers and $j = \ell \pm \frac{1}{2}$, when a hole is created in shell or subshell $n'l'j'$, within the sudden approximation approach, is given by

$$Q_{n'l'j'}(n\ell j) = 1 - [|\langle\psi_{n\ell j}(A^+)|\psi_{n\ell j}(A)\rangle|^2]^N - P_{\rm F}, \qquad (3)$$

where $|\psi_{n\ell j}(A)\rangle$ and $|\psi_{n\ell j}(A^+)\rangle$ stand, respectively, for the orbitals $n\ell j$ of the neutral atom and the orbital $n\ell j$ in the ion A^+ whereby a single vacancy has been created in a subshell $n'l'j'$ of atom A. N is the number of electrons in subshell $n\ell j$.

The condition that electron shake-up transitions to occupied levels are not physically allowed is expressed by the correction $P_{\rm F}$. The correction for contributions to filled states (from $n' = 1$ to x) is

$$P_{\rm F} = \sum_{n'=1}^{n'=x} \frac{NN'}{2j+1} |\langle\psi_{n'\ell j}(A^+)|\psi_{n\ell j}(A)\rangle|^2, \qquad (4)$$

where $n' \neq n$, and N' is the number of electrons in the subshell $n'\ell j$

In this work the M-subshell electron shake-off plus shake-up probabilities, $[KM]$, as the result of single K-shell

TABLE II. The averaged fitting parameters for the $K\beta_{1,3}$ spectra from the elements Ca to Mn using four or five symmetric Lorentzians. Intensity ratios are normalized. Uncertainties are indicated within parentheses. All specimens are metallic, except for Ca. In this case a CaF_2 specimen was used. For all presented cases the primary target was Rh and the spectrometer crystal was Si(220)×2.

	Line	Energy (eV)	Int. ratio
Ca ($Z = 20$)	Line	Energy (eV)	Int. ratio
	$K\beta_{1,3}$	4012.644(22)	100
	$K\beta'$	4008.83(12)	2.37(20)
	$K\beta''$	4016.598(35)	6.67(15)
	$K\beta_5$	4029.454(49)	4.113(71)
Sc ($Z = 21$)	$K\beta_1$	4460.609(25)	76.0(1.7)
	$K\beta_3$	4459.757(34)	62.3(5.5)
	$K\beta'_1$	4458.553(44)	100
	$K\beta'_2$	4448.46(11)	9.29(18)
	$K\beta''$	4464.341(19)	4.57(15)
	$K\beta_5$	4486.063(65)	3.191(34)
Ti ($Z = 22$)	$K\beta_1$	4931.953(75)	100
	$K\beta_3$	4391.034(88)	55.7(4.7)
	$K\beta'_1$	4929.324(89)	84.7(4.3)
	$K\beta'_2$	4924.45(15)	70.5(1.3)
	$K\beta''$	4935.702(79)	0.98(14)
	$K\beta_5$	4961.545(29)	6.65(25)
V ($Z = 23$)	$K\beta_1$	5427.416(50)	100
	$K\beta_3$	5426.460(74)	45.2(7.4)
	$K\beta'_1$	5424.301(26)	57.6(4.5)
	$K\beta'_2$	5417.829(87)	72.5(3.3)
	$K\beta_5$	5461.591(55)	5.73(33)
Cr ($Z = 24$)	$K\beta_1$	5946.758(42)	100
	$K\beta_3$	5945.556(46)	52.6(3.3)
	$K\beta'_1$	5942.497(38)	38.7(3.4)
	$K\beta'_2$	5936.09(19)	72.8(1.8)
	$K\beta_5$	5985.814(37)	5.889(49)
Mn ($Z = 25$)	$K\beta_1$	6490.57(11)	100
	$K\beta_3$	6489.17(13)	50.1(4.2)
	$K\beta'_1$	6485.45(23)	36.3(6.8)
	$K\beta'_2$	6478.30(19)	71.8(2.3)
	$K\beta_5$	6534.54(18)	4.37(25)
Fe ($Z = 26$)	$K\beta_1$	7059.989(66)	100
	$K\beta_3$	7056.21(19)	53.5(4.8)
	$K\beta'_1$	7052.70(55)	28.6(5.7)
	$K\beta'_2$	7045.97(20)	71.8(4.9)
	$K\beta_5$	7108.413(56)	4.10(24)
Co (Z = 27)	$K\beta_1$	7649.498(71)	100
	$K\beta_3$	7647.115(92)	53.6(3.8)
	$K\beta'$	7639.75(12)	61.7(2.2)
	$K\beta''$	7653.726(69)	2.07(59)
	$K\beta_5$	7705.008(81)	2.65(14)
Ni ($Z = 28$)	$K\beta_1$	8264.98(14)	100
	$K\beta_3$	8262.90(16)	78.(14.)
	$K\beta'_1$	8256.52(22)	59.6(7.3)
	$K\beta''_1$	8267.49(28)	16.2(4.7)
	$K\beta''_2$	8270.00(34)	7.8(2.6)
	$K\beta_5$	8327.45(24)	2.73(34)
Cu ($Z = 29$)	$K\beta_1$	8905.35(11)	100
	$K\beta_3$	8902.97(12)	59.6(3.7)
	$K\beta'_1$	8898.849(95)	39.6(1.4)
	$K\beta''_1$	8908.26(14)	24.6(2.5)
	$K\beta''_2$	8911.31(25)	7.6(1.4)
	$K\beta_5$	8976.84(18)	1.968(92)
Zn ($Z = 30$)	$K\beta_1$	9572.234(26)	100
	$K\beta_3$	9569.322(18)	48.2(1.9)
	$K\beta'$	9565.03(16)	16.9(1.5)
	$K\beta''$	9576.439(84)	20.18(90)
Ge ($Z = 32$)	$K\beta_1$	10982.169(17)	100
	$K\beta_3$	10977.961(11)	44.9(2.8)
	$K\beta'_1$	10975.24(20)	11.9(3.2)
	$K\beta''_1$	10988.193(84)	8.08(57)
	$K\beta_5$	11099.732(45)	3.03(98)

ionization have been calculated in the SA model [Eq. (3)] using the MCDF wave functions [41] for the neutral atom (initial state) and for the ion with a single 1*s* hole (final state), for selected atoms with $20 \leqslant Z \leqslant 32$.

TABLE III. The corrected FWHM (CF), in eV, and the lifetime linewidths computed in this work (Theory) using the MCDFGME code, for the $K\beta_{1,3}$ x-ray diagram lines, are presented for elements Ca to Ge, respectively. For Ni there are two calculated values for each linewidth, depending on the ground-state configuration (see text for explanation).

	$K\beta_1$ linewidth			$K\beta_3$ linewidth		
	CF	Theory	Other	CF	Theory	Other
Ca ($Z = 20$)			1.97[a]			1.97[a]
Sc ($Z = 21$)	1.007(23)		1.04(4)[b]	1.630(95)		1.85(10)[b]
			2.03[a]			2.03[a]
						0.93[b]
Ti ($Z = 22$)	1.200(20)	1.02	2.09[a]	1.73(12)	1.17	2.09[a]
V ($Z = 23$)	1.448(32)		2.16[a]	2.08(13)		2.16[a]
Cr ($Z = 24$)	1.611(25)		2.22[a]	2.45(11)		2.22[a]
Mn ($Z = 25$)	1.899(43)		2.31[a]	2.78(24)		2.31[a]
Fe ($Z = 26$)	2.251(43)		2.42[a]	3.14(24)		2.42[a]
Co ($Z = 27$)	2.838(66)		2.55[a]	4.19(18)		2.53[a]
			3.05(1)[c]			3.58(3)[c]
Ni ($Z = 28$)	2.97(19)	.57 (^{3}F)	2.69[a]	4.03(15)	.70 (^3F)	2.69[a]
		.31 (^3D)	3.76(2)[c]		.14 (^3D)	4.34(3)[c]
Cu ($Z = 29$)	3.20(13)	4.60	3.29[a]	3.47(12)	4.64	3.29[a]
			3.52(1)[c]			3.52(1)[c]
			3.29[d]			3.29[d]
			3.25[d]			3.25[d]
Zn ($Z = 30$)	3.59(19)	4.98	3.72[a]	3.56(23)	5.02	3.72[a]
Ge ($Z = 32$)	4.20(51)	4.94	4.22[a]	4.13(17)		

[a]Campbell and Papp [42].
[b]Anagnostopoulos *et al.* [10].
[c]Hölzer *et al.* [5].
[d]Pham *et al.* [15].

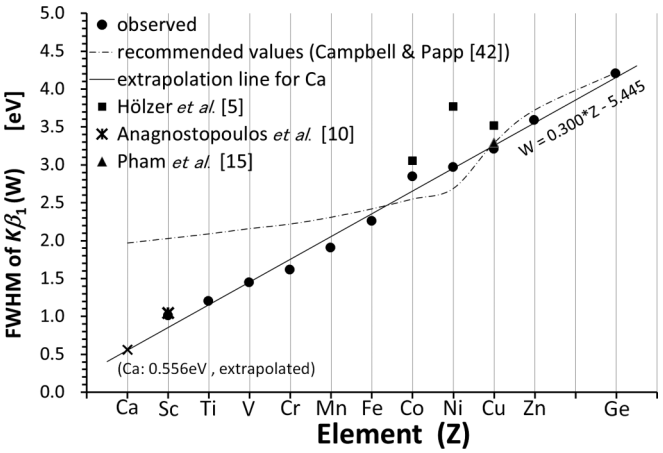

FIG. 3. The corrected FWHM (CF) of the $K\beta_1$ line of elements Ca to Ge together with the recommended values reported by Campbell and Papp [42]. The width of the Ca $K\beta_1$ line was obtained by extrapolating the linear function by the least-squares method using $K\beta_1$ linewidths.

IV. RESULTS AND DISCUSSION

A. The observed $K\beta_{1,3}$ emission spectra

The $K\beta_{1,3}$ spectra of elements Ca to Ge have been measured three times each, using a high-resolution double-flat crystal x-ray spectrometer. The values of the obtained averaged line energies and averaged relative intensity ratios for each line in each Lorentzian model, for Ca, Sc, Ti, Cr, Mn, Fe, Co, Ni, Zn, and Ge, are shown in Table II. The corrected FWHM (CF) for the $K\beta_1$ and $K\beta_3$ diagram lines are presented in Table III, and Figs. 3 and 4, respectively, together with values reported by other authors. The CF values were taken from the observed FWHM through Tochio's method [20]. Table III shows also the lifetime linewidths, calculated in this work using the MCDFGME code. The latter values do not include the spread in energy due to the multiplicity of initial and final transition levels.

For Ni, we present two values for each linewidth, depending on its ground-state configuration. Although the lowest energy level of Ni is [Ar]$3d^8 4s^2\ ^3F_4$, the [Ar]$3d^9 4s\ ^3D_4$ level stands

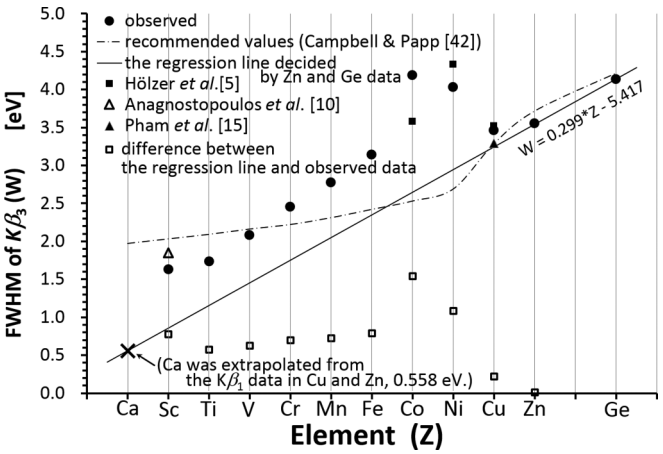

FIG. 4. CF of the $K\beta_3$ line of elements Ca to Ge is shown together with the recommended values [42].

TABLE IV. Measured and calculated K$\beta_{1,3}$ x-ray diagram lines spin doublet energies for Ca to Ge, and values obtained by other authors.

	$K\beta_{1,3}$ split			
	This work, Exp	This work, Th		Other
		MCDFGME	GRASP	
Ca ($Z = 20$)		0.38	0.26	0.27[a]
Sc ($Z = 21$)	0.852(12)			0.39[a]
Ti ($Z = 22$)	0.919(18)			0.54[a]
V ($Z = 23$)	0.957(73)			0.71[a]
Cr ($Z = 24$)	1.202(12)			0.91[a]
Mn ($Z = 25$)	1.403(74)			1.15[a]
Fe ($Z = 26$)	1.695(70)	2.46		1.44[a]
Co ($Z = 27$)	2.383(54)			1.77[a]
				1.77[c]
Ni ($Z = 28$)	2.078(48)	1.81		2.11[a]
				2.00[b]
Cu ($Z = 29$)	2.381(19)	2.51	2.30	2.49[a]
				2.42[d]
				2.56[c]
Zn ($Z = 30$)	2.912(19)	3.02	2.82	3.24[a]
Ge ($Z = 32$)	4.208(13)			

[a]Misra *et al.* [43].
[b]G. Hölzer *et al.* [5].
[c]Pham *et al.* [15].

only 0.0254 eV above the ground energy, which means that in experiments at room temperature that level will certainly be highly populated. The uncertainties associated to the calculated linewidths are dominated by the uncertainties in the K-level widths. These were estimated by comparing the MCDFGME results for the radiative transitions in the length and velocity gauges and assuming they are of the same order for the radiationless transitions. With this approach the uncertainty was found to be about 2%.

The $K\beta_{1,3}$ spin doublet values observed and calculated in this work are presented in Table IV and Fig. 6, together with other observed values [4,5,10] and the recommended values based on the experimental results of Campbell and Papp [42], the values obtained from a refinement of the modified Moseley plot method by Misra *et al.* [43], and Pham *et al.* [15]. The Lorentzian model was used for an analytic representation of $K\beta$ x-ray lines [4,14], and the results of the fitting analyses are shown in Fig. 1 for elements from Ca to Mn, and in Fig. 2 for elements from Fe to Zn, and Ge. (The atomic data and the spectral diagram of Ni $K\beta_{1,3}$ were independently measured and analyzed from Menésguen *et al.* [44]. In the $3d$ $K\beta_{1,3}$ spectral analysis, we referred to their method.) The errors quoted in Table II are thus only statistical errors resulting from the fitting processes and the limited reproducibility of the experimental setup. To obtain realistic uncertainties, the errors originating from the energy calibration have to be considered. Absolute $K\beta_{1,3}$ photon energies for all $3d$ elements between Cr and Cu can be found in Refs. [5] and [45].

The search for a physical interpretation of the line characteristic parameter (such as the width, asymmetry index, etc.) dependence on Z over a wide Z range has been the object of several works [4,5,10]. The FWHM and the intensity ratio in

$K\beta$ lines constitute the basis of a well-known identification of the line shape. The values obtained in this work for these two quantities allow for a comparison with other experimental results and to other reference data. We note, however, that, as also suggested by Hölzer *et al.* [5], a precise description of the line shape by a simple asymmetric profile is not possible in all cases, including the $K\beta$ lines. Also, complete corrections for the instrumental broadening have not been included in width values obtained in several measurements on $3d$ elements [5]. The double-crystal spectrometer setup has the advantage of allowing for the determination of the emission line true FWHM by a simple subtraction of the convolution in the crystal dispersion from the FWHM of the measured emission line [20]. This approach was employed in this work.

In Fig. 3 we can see that the overall variation behavior with Z of the CF of the $K\beta_1$ line, as a function of Z, may be linearly fitted with the function $W = 0.300 \times Z - 5.445$ and, using this function, the corrected Ca $K\beta_1$ spectral line FWHM, 0.556 eV, was obtained, as seen in Fig. 3.

As seen in Fig. 4, the CF values of the $K\beta_3$ lines are very different from those of the $K\beta_3$ from Campbell and Papp [42], although the values are consistent with the latter for the elements Cu to Ge. As the Ca $K\beta_3$ CF could not be obtained using the fitting method, this value was found by the extrapolation of the linear function obtained by the least-squares method from the $K\beta_3$ emission lines values in the elements Zn and Ge. Its FWHM was found to be 0.558 eV. These values are in good agreement with each other.

From the difference of CF values in $K\beta_{1,3}$ diagram lines, we considered that the change of the FWHM in the $K\beta_3$ spectra from elements Sc to Ni, could be ascribed to the M_2-$M_{4,5}M_{4,5}$ and M_3-$M_{4,5}M_{4,5}$, or M_2-$M_3M_{4,5}$ super–Coster-Kronig transitions, as seen in Fig. 4. However, according to our theoretical calculations, M_2-$M_3M_{4,5}$ super–Coster-Kronig transitions are possible only for elements from Ti to Fe and their widths are very small, i.e., in the range of 0.006–0.015 eV. The results of our detailed theoretical calculations of M_2-$M_{4,5}M_{4,5}$ and M_3-$M_{4,5}M_{4,5}$ super–Coster-Kronig transitions for all studied elements from Sc to Ge, obtained using DFS method in the framework of the FACpackage, are presented in Fig. 5. However, these results also do not explain fully the change of the FWHM in the $K\beta_3$ spectra from Sc to Ni.

Using the FWHM of the Zn and Ge $K\beta_3$ line, the Ca $K\beta_3$ linewidth was obtained, and its value was almost the same as that of the Ca $K\beta_1$ linewidth. The difference between the observation and the value extrapolated is around 0.5 eV from Sc to Ni. Around the Co $K\beta_3$ line, there is a maximum in the width. The difference is not clear yet.

It is worth noting that Lorentzian shapes for diagram and satellite lines were applied for the systematic analysis of all studied elements. In the case of Cu, we assumed that the $K\beta'$ and $K\beta''$ satellite lines are attributed to the $[KM]$ shake contribution, following Ref. [4]. Therefore in this paper the transition probability values for $[KM]$ shake double excitation, as the result of single K-shell ionization, have been calculated in the SA model for Cu and all other studied elements. Moreover, the correspondence between observed and predicted $K\beta_{1,3}$ x-ray spectra has been investigated and is presented in Sec. IV B.

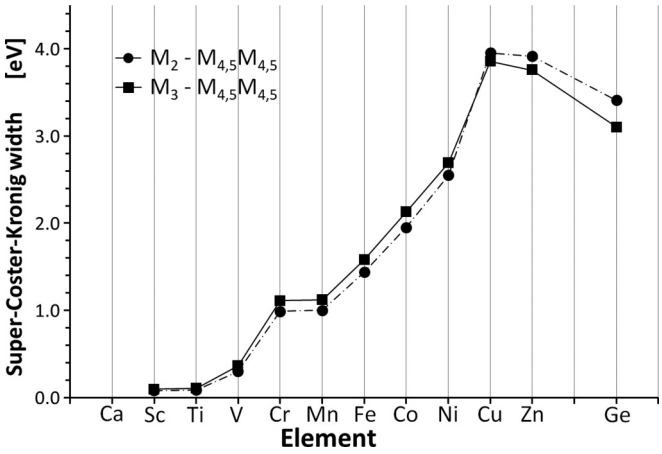

FIG. 5. The results of theoretical calculations of M_2-$M_{4,5}M_{4,5}$ and M_3-$M_{4,5}M_{4,5}$ super–Coster-Kronig transitions for elements from Sc to Ge, obtained using the DFS method in the framework of the FAC package.

More recently, Pham *et al.* [15] and Lowe *et al.* [46] pointed out that these deviations were ascribed to the unique electronic structure of the atoms in the elements with a fully populated $4s$ and an open $3d$ subshell, leading to excitation dynamics in the x-ray emission process. In particular, the number of unpaired electrons is maximal for Mn, which corresponds well to the experimentally observed change in the satellite intensity, as seen in Fig. 1. Details of the theoretical approaches can be found in Sec. IV B.

From the fitting analysis of $K\beta_{1,3}$ spectra in $3d$ elements, each $K\beta_{1,3}$, $K\beta'$, and $K\beta''$, etc., peak energy, was obtained as seen in Table II. Also, the observed split energy values between $K\beta_1$ and $K\beta_3$ spectra in Table IV are shown in Fig. 6. The split energy is represented by the function of $\log_{10} S = 0.0642 \times (Z - 24.886\,17) + 0.1491$ as seen in Fig. 6. At the present time, the physical meaning of this function is not clarified.

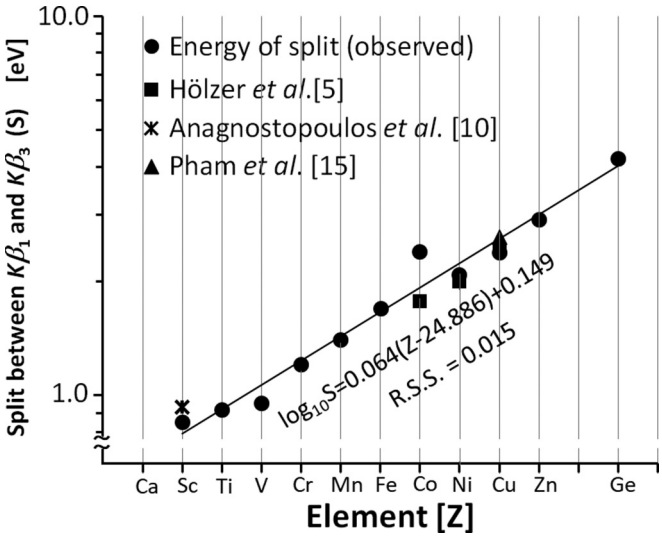

FIG. 6. The spin doublet energies of $K\beta_1$ and $K\beta_3$ lines for elements Sc to Ge. The least-squares fitting was executed using both data in the present work.

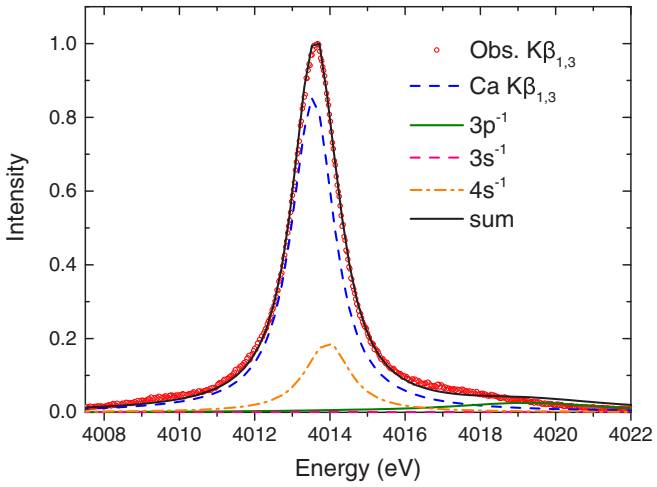

FIG. 7. Comparison of the high-resolution experimental spectra with the predicted $K\beta_{1,3}$ spectra of Ca including the contributions of the $K\beta_{1,3}$ diagram lines and the satellite lines (in different colors, identified in the legend) for $[1s3p]$, $[1s3s]$, and $[1s4s]$ hole states.

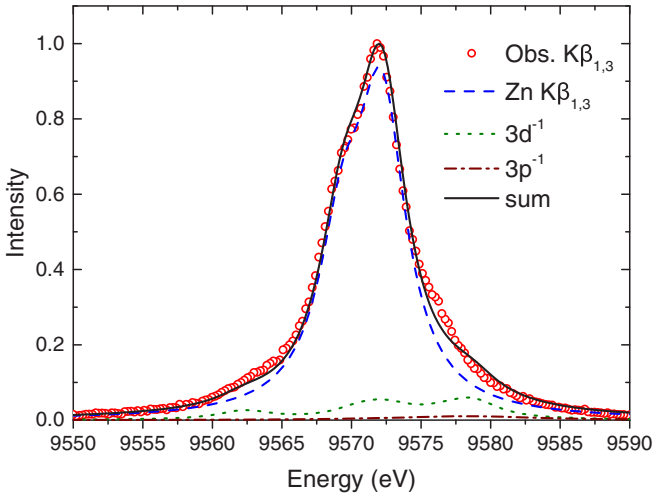

FIG. 8. Similarly as in Fig. 7, but for Zn, with the $3d^{10}4s^2$ valence configuration in the ground state.

In what concerns the accuracy of our MCDF predictions, we estimate that the precision for the calculated values for the positions of the $K\beta_1$ and $K\beta_3$ x-ray diagram lines is in the order of 0.1–0.2 eV. Moreover, some of the approximations included in the code tend to affect both energy values in a similar way, so that their effect may partly disappear from differences such as energy shifts. Therefore, we can also expect that the precision of our simulations for diagram and satellite line shapes and positions should also be high.

B. Comparison of experimental $K\beta_{1,3}$ x-ray spectra with theoretical predictions based on the shake processes for Ca, Mn, Cu, and Zn elements

In order to unravel the origin of the experimental spectra shapes, the theoretically predicted $K\beta_{1,3}$ x-ray spectra for Ca, Mn, Cu, and Zn elements, obtained as a superposition of different contributions corresponding to diagram and satellite lines by using probabilities of shake processes, have been compared with the experimental ones (see Figs. 7–10). The synthesized spectra for all diagram and satellite line contributions of $K\beta_{1,3}$ x-ray spectra are the sum of the individual transitions, assuming for each a Lorentzian line shape with specific FWHM.

In the case of all analyzed elements we have found that for all predicted diagram lines to reproduce well the shape of the $K\beta_{1,3}$ x-ray experimental spectra, we needed to slightly modify the specific linewidths provided on the basis of Campbell and Papp data [42]. Thus, for the $K\beta_{1,3}$ x-ray diagram lines of Ca, Mn, Cu, and Zn, we have obtained from our modeling the following linewidths: 1.3, 1.8, 4.1, and 4.2 eV, respectively. For the satellite lines we have calculated the linewidths from the recommended level values of Campbell and Papp [42]. Therefore, for the $[1s3p]$ satellite lines of Ca, Mn, Cu, and Zn the linewidths found are 3.7, 4.2, 7.7, and 8.4 eV, respectively. In turn, for Mn, Cu, and Zn, the obtained values for the $[1s3d]$ satellite linewidths are 1.8, 4.1, and 4.2 eV, respectively. Moreover, for the $[1s3s]$ and $[1s4s]$ satellite linewidths of Ca we have obtained 3.6 and 1.3 eV, respectively. Corrections for the instrumental broadening have not been included in our predictions.

In this work, the electron shake-off plus shake-up probabilities as the result of single K-shell ionization have been calculated in the SA model, Eq. (3), using MCDF wave functions [41] for the neutral atom (initial state) and for the ion with a single $1s$ hole (final state), for atoms with $20 \leqslant Z \leqslant 32$. For clarity of our discussion we have considered two kinds of elements, characterized by radically different valence electron configurations in the neutral atom ground states, i.e., the elements with closed-shell configurations, such as Ca ([Ne] $3s^2 3p^6 4s^2$) and Zn ([Ne] $3s^2 3p^6 3d^{10} 4s^2$), and elements with open-shell configurations, such as Mn ([Ne] $3s^2 3p^6 3d^5 4s^2$). Here [Ne] means the electronic configuration of the neon atom.

First we have compared the theoretically predictions for closed-shell configurations in the case of elements Ca (Fig. 7) and Zn (Fig. 8). For Ca, the relative intensities for diagram and each satellite lines (i.e., peak areas) have been evaluated taking into account the results of the shake-off and shake-up

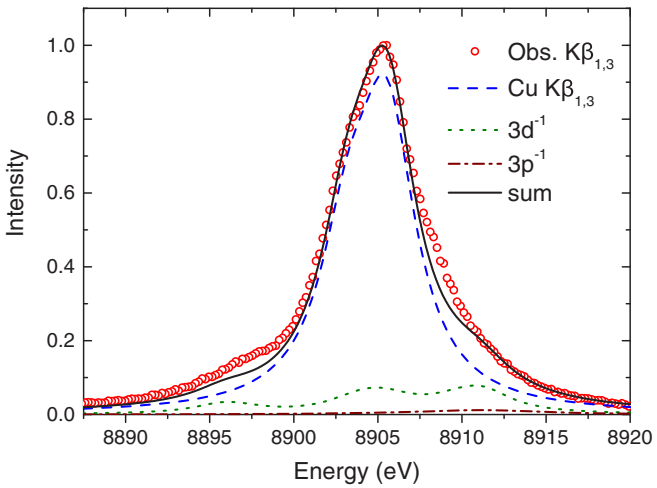

FIG. 9. Similarly as in Figs. 7 and 8, but for Cu, with the $3d^{10}4s$ valence configuration in the ground state.

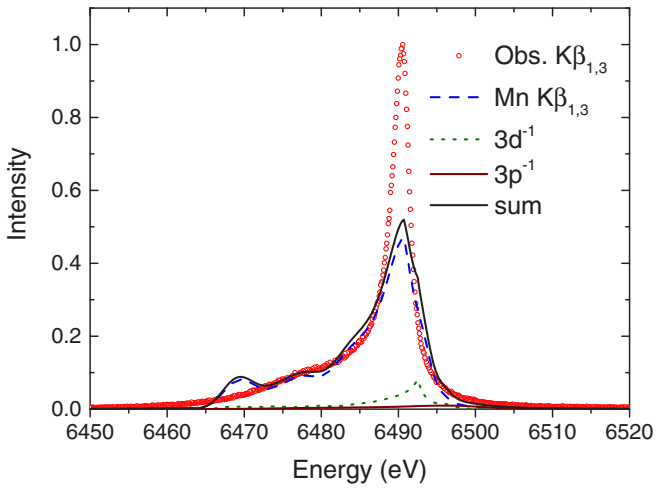

FIG. 10. Comparison of the high-resolution experimental spectra with predicted $K\beta_{1,3}$ spectra for Mn with the $3d^5 4s^2$ open-shell valence configuration, including the contributions from the $K\beta_{1,3}$ diagram lines, and satellite lines (in different colors, identified in the legend) predicted on the basis of the $[1s3d]$ and $[1s3p]$ shake-process probabilities.

probabilities for production of $[1s3p]$, $[1s3s]$, and $[1s4s]$ hole states.

In the case of Zn, the relative intensities for diagram and each satellite line have been obtained using the results of the shake-off and shake-up probabilities for production of $[1s3d]$ and $[1s3p]$ hole states. As can be seen, for elements Ca and Zn, with closed-shell valence configurations in ground state, our theoretical predictions reproduce very well (Figs. 7 and 8) the high-resolution experimental data.

We should emphasize that in the case of the $3d$ transition metals the shape of the $K\beta_{1,3}$ x-ray spectra is determined by the number of electrons in the $3d$ shell. Therefore, for Cu (Fig. 9), with the configuration [Ne] $3s^2 3p^6 3d^{10} 4s^1$ in the ground state, the situation is very similar to Zn (Fig. 8). As can be seen, our theoretically predicted synthesized spectrum presented in Fig. 9 is also in very good agreement with the high-resolution experimental one.

Much more complicated is the case of Mn $K\beta_{1,3}$ x-ray spectra, presented in Fig. 10, where the so called open-shell valence configuration (OVC) effect [45,47] exists. This figure shows the predicted $K\beta_{1,3}$ diagram lines and the satellite lines presented in different colors, obtained on the basis of the shake-process probabilities, together with the observed ones. Due to the $3d^5 4s^2$ open-shell valence configuration in the neutral Mn ground state, there are, for each transition type, many initial and final states. In this element, even considering diagram lines alone, the $K\beta_{1,3}$ spectrum consists of numerous overlapping components (7429 transitions) having different energies. As a consequence of the OVC effect, the effective natural line shapes in Mn, even considering only diagram lines, have already a very rich structure with visible asymmetry. The $[1s3d]$ and $[1s3p]$ satellite lines are also a source of further complicated structures, because more than 100 000 transitions appear. The very rich theoretical structure of Mn $K\beta_{1,3}$ lines, together with the complicated structure of the experimental metallic Mn, are the main sources of the discrepancy between the experimental results and the theoretical $K\beta_{1,3}$ spectrum presented in Fig. 10. However, despite that, our theoretical spectrum is in moderate agreement with the experimental one and explains the shape of main part of the very-high-resolution experimental spectrum.

From these calculations, we may conclude that the $K\beta'$ and $K\beta''$ peaks result mainly from the $[KM]$ shake process, proving that these peaks do not correspond to diagram lines.

V. SUMMARY AND CONCLUSIONS

We measured and analyzed systematically the $K\beta_{1,3}$ x-ray spectra in elements from Ca to Ge using a double-crystal x-ray spectrometer, considering from the theoretical point of view the electronic transitions.

The natural linewidths and the relative intensities of the diagram lines, $K\beta'$ and $K\beta''$ satellite lines in the elements from Ca to Ge have been evaluated from the measurements of the $K\beta_{1,3}$ x-ray spectra. The averaged corrected FWHM values of the $K\beta_1$ emission x-ray line in these elements increases linearly with Z. However, the FWHM of the $K\beta_3$ line seem to be larger by around 0.5 eV than the FWHM values of $K\beta_1$ line, for elements between Sc and Ni, and when compared with the values obtained from the least-squares fitting using Ge and Zn values [13,48]. The difference in FWHM between $K\beta_1$ and $K\beta_3$ x-ray lines for the studied elements is not clear yet.

The spin doublet of $K\beta_1$ and $K\beta_3$ spectra was obtained systematically in the $3d$ elements. These experimental values are well represented by the exponential function used in the fitting process.

Contrary to what can be observed in Ca and Zn, with a closed-shell structure, and Cu with only one hole, in the $4s$ shell, the theoretical prediction of the Mn $K\beta_{1,3}$ line shape is not in full agreement with the measured one. This is most probably due to OVC effects and the fact that the five $3d$ electrons in Mn are much more involved in the chemical bonding of the metallic sample complicated structure than in Cu or Zn. This fact will lead to changes in the orbital energies and even in the transition selection rules, which in turn will lead to changes in the individual transition rates and yields [49]. The presence of thin oxide layers in the metallic samples can also induce chemical shifts in the orbital energies which may have a sizable effect in the line shapes, as has been observed by Mukoyama *et al.* [50,51].

We believe that the results of research presented here constitute not only a valuable basis for the interpretation of the structure of high-resolution $K\beta_{1,3}$ x-ray spectra for the elements from Ca to Ge, but they also may be a motivation for planning new measurements of $K\beta_{1,3}$ x-ray emission spectra of $3d$ transition metals.

ACKNOWLEDGMENTS

Y.I. acknowledges financial support for the measurements of a part of the data by the REXDAB Collaboration that was initiated within the International Fundamental Parameter Initiative. This work is supported also in part by the Polish National Science Center under Grant No. 2011/01/D/ST2/01286. This work was funded partly by the Portuguese Foundation for Science and Technology (FCT)

under Projects No. UID/MULTI/04046/2013 (BioISI) and No. UID/FIS/04559/2013 (LIBPhys). Laboratoire Kastler Brossel (LKB) is "Unité Mixte de Recherche du CNRS, de l'ENS et de Sorbonne Université No. 8552." We also thank the Allianz Program of the Helmholz Association, Contract No. EMMI HA-216, "Extremes of Density and Temperature: Cosmic Matter in the Laboratory." M.G. acknowledges the support of FCT (Portugal) under Contract No. SFRH/BPD/92455/2013.

[1] J. Finster, G. Leonhardt, and A. Meisel, J. Phys. Colloques **32**, C4-218 (1971).
[2] B. Ekstig, E. Källne, E. Noreland, and R. Manne, J. Phys. Colloques **32**, C4-214 (1971).
[3] M. Pessa, E.-K. Kortela, A. Suikkanen, and E. Suoninen, Phys. Rev. A **8**, 48 (1973).
[4] M. Deutsch, G. Hölzer, J. Härtwig, J. Wolf, M. Fritsch, and E. Förster, Phys. Rev. A **51**, 283 (1995); M. Deutsch, O. Gang, G. Hölzer, J. Härtwig, J. Wolf, M. Fritsch, and E. Förster, *ibid.* **52**, 3661 (1995).
[5] G. Hölzer, M. Fritsch, M. Deutsch, J. Härtwig, and E. Förster, Phys. Rev. A **56**, 4554 (1997).
[6] M. J. Druyvesteyn, Z. Phys. **43**, 707 (1927); Ph. D. Thesis, University of Groningen (1928), (unpublished).
[7] D. Doniach and M. Šunjić, J. Phys. C **3**, 285 (1970).
[8] K. Tsutsumi and H. Nakamori, in *X-ray Spectra and Electronic Structure of Matter*, edited by A. Faessler and G. Wiech (Fotodruck Frank OHG, Munchen, 1973); K. Tsutsumi, J. Phys. Soc. Jpn. **14**, 1696 (1959); K. Tsutsumi, Y. Iwasaki, O. Aita, K. Ichikawa, and T. Watanabe, *ibid.* **47**, 1920 (1979); S. I. Salem, G. M. Hockney, and P. L. Lee, Phys. Rev. A **13**, 330 (1976).
[9] K. S. Srivastava, R. L. Shrivastava, O. K. Harsh, and V. Kumar, Phys. Rev. B **19**, 4336 (1979); K. S. Srivastava, S. Singh, A. K. Srivastava, R. S. Nayal, A. Chaubey, and P. Gupta, Phys. Rev. A **25**, 2838 (1982).
[10] D. F. Anagnostopoulos, R. Sharon, D. Gotta, and M. Deutsch, Phys. Rev. A **60**, 2018 (1999).
[11] C. T. Chantler, M. N. Kinnane, C.-H. Su, and J. A. Kimpton, Phys. Rev. A **73**, 012508 (2006).
[12] Y. Ito, T. Tochio, H. Oohashi, and A. M. Vlaicu, Radiat. Phys. Chem. **75**, 1534, (2006).
[13] Y. Ito, T. Tochio, H. Ohashi, M. Yamashita, S. Fukushima, M. Polasik, K. Słabkowska, Ł. Syrocki, E. Szymańska, J. Rzadkiewicz, P. Indelicato, J. P. Marques, M. C. Martins, J. P. Santos, and F. Parente, Phys. Rev. A **94**, 042506 (2016).
[14] T. Ishizuka T. Tochio, A. M. Vlaicu, D. Osawa, Y. Ito, T. Mukoyama, S. Hayakawa, Y. Gohshi, and T. Shoji, Advances in X-Ray Chemical Analysis, Japan **30**, 21 (1998).
[15] T. L. H Pham, T. V. B Nguyen, J. A. Lowe, I. P. Grant, and C. T. Chantler, J. Phys. B **49**, 035601 (2016).
[16] W. C. Sauder, J. R. Huddle, J. D. Wilson, and R. E. LaVilla, Phys. Lett. A **63**, 313 (1977).
[17] R. E. LaVilla, Phys. Rev. A **19**, 717 (1979); J. Bremer and H. Sørum, Phys. Lett. A **75**, 47 (1979).
[18] R. D. Deslattes, R. E. LaVilla, and A. Henins, Nucl. Instrum. Methods **152**, 179 (1978).
[19] S. P. Limandri, A.C. Carreras, R.D. Bonetto, and J.C. Trincavelli, Phys. Rev. A **81**, 012504 (2010).
[20] T. Tochio, Y. Ito, and K. Omote, Phys. Rev. A **65**, 042502 (2002).
[21] J. A. Bearden, Rev. Mod. Phys. **39**, 78 (1967).
[22] I. P. Grant, Int. J. Quantum Chem. **25**, 23 (1984).
[23] K. G. Dyall, I. P. Grant, C. T. Johonson, F. A. Parpia, and E. P. Plummer, Comput. Phys. Commun. **55**, 425 (1989).
[24] M. Polasik, Phys. Rev. A **39**, 616 (1989); **39**, 5092 (1989); **40**, 4361 (1989); **41**, 3689 (1990); **52**, 227 (1995); **58**, 1840 (1998).
[25] F. A. Parpia, C. F. Fischer, and I. P. Grant, Comput. Phys. Commun. **94**, 249 (1996).
[26] P. Jönsson, X. He, C. F. Fischer, and I. P. Grant, Comput. Phys. Commun. **177**, 597 (2007).
[27] C. Froese Fischer and G. Gaigalas, Phys. Rev. A **85**, 042501 (2012).
[28] J. P. Desclaux, Comput. Phys. Commun. **9**, 31 (1975).
[29] P. Indelicato, Phys. Rev. A **51**, 1132 (1995).
[30] M. F. Gu, Astrophys. J. **582**, 1241 (2003).
[31] M. F. Gu, Can. J. Phys. **86**, 675 (2008).
[32] E. L. Feinberg, J. Phys. (USSR) **4**, 423 (1941).
[33] A. Migdal, J. Phys. (USSR) **4**, 449 (1941).
[34] T. A. Carlson and J. C. W. Nestor, Phys. Rev. A **8**, 2887 (1973).
[35] T. A. Carlson, Phys. Rev. **156**, 142 (1967).
[36] T. A. Carlson, C. W. Nestor, Jr., T. C. Tucker, and F. B. Malik, Phys. Rev. **169**, 27 (1968).
[37] M. O. Krause and T. A. Carlson, Phys. Rev. **158**, 18 (1967).
[38] V. P. Sachenko and E. V. Burtsev, Bull. Acad. Sci. USSR, Phys. Ser. **1**, 980 (1968).
[39] J. P. Santos, M. F. Laranjeira, and F. Parente, Europhys. Lett. **55**, 479 (2001).
[40] O. Mauron, J.-Cl. Dousse, S. Baechler, M. Berset, Y.-P. Maillard, P.-A. Raboud, and J. Hoszowska, Phys. Rev. A **67**, 032506 (2003).
[41] O. Mauron, J.-Cl. Dousse, J. Hoszowska, J. P. Marques, F. Parente, and M. Polasik, Phys. Rev. A **62**, 062508 (2000).
[42] J. L. Campbell and T. Papp, At. Data Nucl. Data Tables **77**, 1 (2001).
[43] U. D. Misra, Meeta Sah, and B. G. Gokhale, J. Phys. B **25**, 4107 (1992).
[44] Y. Menesguen, M.-C. Lepy, P. Honicke, M. Muller, R. Unterumsberger, B. Beckhoff, J. Hoszowska, J.-C. Dousse, W. Blachucki, Y. Ito, M. Yamashita, and S. Fukushima, Metrologia **55**, 56 (2017).
[45] Y. Ito, T. Tochio, and S. Fukushima (unpublished).
[46] J. A. Lowe, C. T. Chantler, and I. P. Grant, Phys. Rev. A **83**, 060501(R) (2011).
[47] M. Polasik, K. Słabkowska, J. Rzadkiewicz, K. Kozioł, J. Starosta, E. Wiatrowska-Kozioł, J.-Cl. Dousse, and J. Hoszowska, Phys. Rev. Lett. **107**, 073001 (2011).
[48] R. Nyholm, N. Måhrtensson, A. Lebuglet, and U. Axelsson, J. Phys. F **11**, 1727 (1981).
[49] M. Guerra, J. M. Sampaio, F. Parente, P. Indelicato, P. Honicke, M. Muller, B. Beckhoff, J.P. Marques, and J. P. Santos, Phys. Rev. A **97**, 042501 (2018).
[50] T. Mukoyama, K. Taniguchi, and H. Adachi, X-Ray Spectrom. **29**, 426 (2000).
[51] T. Mukoyama, K. Taniguchi, and K. Adachi, Phys. Rev. A **63**, 042514 (2001).